Available online at www.sciencedirect.com
ScienceDirect
Journal of Power Sources 181 (2008) 244–250
JOURNAL OF POWER SOURCES
www.elsevier.com/locate/jpowsour

# The electrochemical cell temperature estimation of micro-tubular SOFCs during the power generation

S. Hashimoto [a,*], H. Nishino [a,1], Y. Liu [a], K. Asano [a], M. Mori [a], Y. Funahashi [b], Y. Fujishiro [c]

[a] Central Research Institute of Electric Power Industry (CRIEPI), 2-6-1 Nagasaka, Yokosuka, Kanagawa 240-0196, Japan
[b] Fine Ceramics Research Association (FCRA), AIST, Shimo-shidami, Moriyama-ku, Nagoya 463-8561, Japan
[c] Advanced Industrial Science and Technology (AIST), Shimo-shidami, Moriyama-ku, Nagoya 463-8561, Japan

Received 3 October 2007; received in revised form 30 November 2007; accepted 19 December 2007
Available online 6 January 2008

**Abstract**

In this study, new temperature monitoring method for solid oxide fuel cells (SOFCs) was proposed, and the demonstration using micro-tubular SOFCs has done. The fabricated micro-tubular SOFCs were operated under the two different conditions, and polarization during the power generation was measured. The cell resistance as a function temperature was also measured. Based on the temperature dependence of cell resistance and the measured ohmic drop during the power generation, the cell temperature was estimated. The estimated cell temperature clearly depended on operation condition and increased with increasing of the current density. The estimated cell temperature was also in nearly proportion to the temperature which was measured by a thermocouple, and it was conformed that this temperature monitoring method by electrochemical technique certainly functioned.


*Keywords:* Solid oxide fuel cells (SOFCs); Micro-tubular cell; Polarization measurement; Temperature management; Ceramic reactor

## 1. Introduction

The solid oxide fuel cells (SOFCs) are one of the promising power generation devices. Although a weak point for SOFCs was previously considered to be startability, Kendall and co-workers [1] reported that micro-tubular SOFCs have high thermal shock resistance and rapid startability. It is now known that small tubular design and lowering operation temperature enable SOFCs to have rapid startability. Since electrode-supported micro-tubular SOFCs can show good performance even at 500–650 °C [2–5], widely applications, which are not only for the stationary but also for the mobile, are expected.

One of the issues for such micro-tubular SOFCs is ohmic loss when collecting current. It was reported that the tubular length and thickness of high performance micro-tubular SOFCs are critical for the cell performance even when Ni–$Ce_{0.8}Gd_{0.2}O_{2-\delta}$ (CGO), which has conductivity of $10^3$ S cm$^{-1}$ or higher, was introduced as a material for the supporting tube [4]. Since such micro-tubular SOFCs are able to generate high power for small cell volume, Joule heat along the current pass will be enhanced. In our previous study, the reduction of ohmic resistance was observed in a micro-tubular SOFC during the power generation [5]. In the experiment, change in ohmic resistance at OCV was not observed before and after the power generation. Therefore, we concluded the ohmic resistance change with the increasing of current was caused by heat generation.

During the power generation of such micro-tubular SOFCs, the heat management will be important issue for the system reliability. The use of thermocouples for temperature monitoring is one of common techniques. However, it does not always reflect actual cell temperature. Especially, in case of the micro-tubular SOFCs, the attachable parts with thermocouples are very limited, and the attachment of thermocouples will be more difficult in stuck or bundle structure. Moreover, the presence of thermocouples will influence the gas flow, temperature balance and so on. Simulation is another important technique to know heat-balance in SOFCs, but it is not for actual cell temperature monitoring.

In this study, we carried out the estimation of cell temperature using electro-chemical technique as a new cell temperature monitoring method for SOFCs. Anode-supported micro-tubular

* Corresponding author. Tel.: +81 46 856 2121; fax: +81 46 856 5571.
*E-mail address:* shinichi@criepi.denken.or.jp (S. Hashimoto).
[1] Present address: Clean Energy Research Center, University of Yamanashi, Japan.

0378-7753/$ – see front matter © 2007 Elsevier B.V. All rights reserved.
doi:10.1016/j.jpowsour.2007.12.104

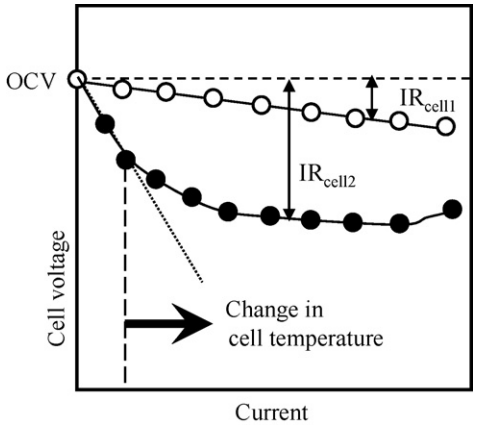


Fig. 1. Cell dependence of change in IR drop during the power generation. Cell 1 (open): low heat-generated cell (no change in the cell temperature). Cell 2 (filled): high heat-generated cell (drastic change in the cell temperature).

SOFCs were operated under the two different conditions. Additionally, polarization during the power generation was measured, and the ohmic loss as a function of current density was confirmed for each condition. Finally, change in cell temperature was estimated based on the temperature dependence of cell resistance and the measured ohmic potential drop during the power generation.

## 2. Electrochemical temperature measurement technique

By polarization measurement, it is possible that the potential drop in the power generation test is divided into two factors, the ohmic potential drop and electrode over-potential [6]. Fig. 1 shows two examples of change in ohmic potential drop during the power generation. It is usually believed that the ohmic potential drop as a function of current (or current density) is linear according to Ohm's law as in the case of cell 1 (open dot) in Fig. 1. However, if the cell resistance is relatively high compared to current level, or the cell structure has difficulty in quick heat radiation, the cell will lose the linearity between ohmic potential drop and current due to change in cell temperature with heat generation (cell 2, filled dots in Fig. 1). It is considered that this change in ohmic potential drop can be applied to cell temperature monitoring.

Fig. 2 shows the schematic diagram of the cell temperature estimation by electrochemical technique. First, polarization of the cell during power generation is measured by impedance method or current interruption method (Fig. 2(a)). The ohmic potential drop as a function of current is obtained and the ohmic resistance at each current is calculated. Secondary, the temperature dependence of the cell resistance at OCV or in low current density region where the ohmic potential drop follows Ohm's law is measured, and the graph as shown in Fig. 2(b) will be plotted. By applying the change in ohmic resistance in Fig. 2(a) and (b), the cell temperature as a function of current will be estimated.

## 3. Experimental

### 3.1. Cell fabrication and cell structure

For the evaluation, anode-supported ScSZ electrolyte microtubular cells were fabricated as shown in Fig. 3(a) [5]. The cell dimensions are 1.8 mm in diameter, 50 mm in length and 1.75 $cm^2$ in cathode area, and the cell configuration was $La_{0.6}Sr_{0.4}Co_{0.2}Fe_{0.8}O_{3-\delta}$ (LSCF)–$Ce_{0.8}Gd_{0.2}O_{2-\delta}$ (CGO) cathode/CGO buffer layer/$(ZrO_2)_{0.89}$–$(Sc_2O_3)_{0.1}$–$(CeO_2)_{0.01}$ (10ScSZ) electrolyte/Ni–10ScSZ anode. CGO buffer layer was formed between the LSCF–CGO cathode and 10ScSZ electrolyte due to better chemical compatibility. Fig. 3(b) shows the reflection electron microscope (REM) image for the cross section of the prepared cell after reducing on the anode. 10ScSZ dense electrolyte layer was successfully formed by co-firing with pore-controlled NiO–10ScSZ substrate tube at 1400 °C. The CGO buffer layer and LSCF–CGO cathode layer were prepared at 1200 °C and 1050 °C, respectively. The CGO buffer layer was not densified, and the average grain size of CGO was ca. 0.2 μm. The thickness of cathode, buffer layer, electrolyte and anode were approximately 30 μm, <1 μm, 10 μm, and 250 μm, respectively.

### 3.2. Electrochemical measurement

The electrochemical measurements have done under two different conditions as shown in Table 1 and Fig. 4. The both ends of the prepared cell were connected to the dedicated cell holder with

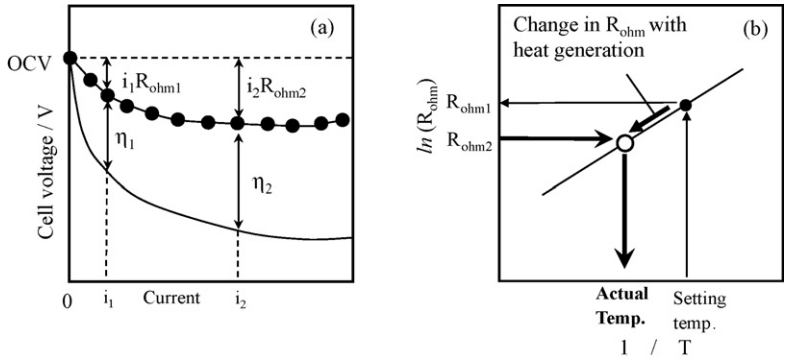


Fig. 2. The cell temperature estimation by electrochemical technique. (a) Step 1: polarization measurement and calculation of ohmic resistance at each current. (b) Step 2: cell temperature estimation from cell ohmic resistance $R_{ohm}$ as a function of temperature.

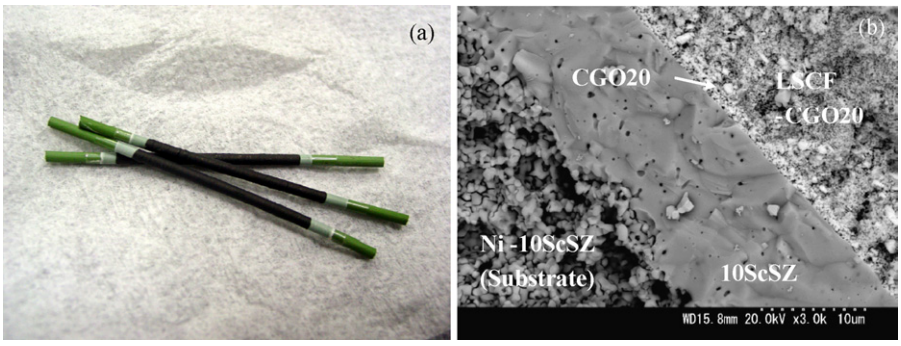


Fig. 3. Test cell structure. (a) Outlook and (b) cross section of the cell observed by reflection electron microscopic (REM) image (after reduction of anode).

Table 1
Measurement conditions

| Conditions | Condition A (open cathode mode) | Condition B (air supply mode) |
|---|---|---|
| Fuel concentration and flow rate | 100% $H_2$, 60 ml $min^{-1}$ | 31% $H_2/N_2$, 145 ml $min^{-1}$ ($H_2$: 45 ml $min^{-1}$; $N_2$: 100 ml $min^{-1}$) |
| Humidify temperature of fuel | Room temperature | ← |
| Air flow rate | Air exposure | 145 ml $min^{-1}$ |
| Current collection (anode side) | Pt wire + Pt paste (partial, only for contacting the wire) | ← |
| Current collection (cathode side) | Cathode material + Pt wire + Ag paste (partial, only for contacting the wire) | Cathode material + Pt paste (all over) + Pt net + Pt wire |

ceramic sealing material (Toagosei, Aron Ceramic C and CC, Japan) for fuel supply to the anode. The cathode was exposed to air in condition A, while air was actively supplied to cathode in condition B. Moreover, better current collection at cathode side was introduced for condition B as shown in Fig. 4. Pt wire twisted around cathode and Ag paste was used only for contacting part between Pt wire and cathode in condition A. On the other hand, Pt paste was applied to the allover the cathode area, and Pt net was bound on the surface using Pt wire in condition B.

The temperature was controlled by a furnace with a PID controller, and the furnace temperature was monitored by a K-type thermo-couple. The setting furnace temperature was previously compensated for the temperature difference from the actual cell setting part. In condition B, another K-type thermo-couple was set near by the micro-tubular cell for cell temperature observation, and the tip of the thermo-couple was located the central part of the cell with ca. 2 mm distance.

The polarization during the power generation was measured by current interruption method [6,7]. A current pulse generator (Nikko-keisoku, NCPG-105S, Japan) was used as a electric load and the pulse source. An electrometer (Hokuto-denko, HC-104, Japan) which has high input resistance, $10^{11}$ Ω, was connected to the potential sensing terminals. Via this electrometer, potential pulse was observed using an oscilloscope (Agilent Technology, DSO3152A, USA), and ohmic drop of the cell was measured.

The cell resistance as a function of temperature was also measured by current interruption method at each condition. To avoid the influence of heat generation, the cell resistance was measured below 100 mA.

## 4. Results and discussion

### 4.1. Power generation and polarization properties under two different conditions

Fig. 5 shows the power generation properties of the developed cell at (a) condition A (open cathode mode) and (b) B (air supply mode). Open circuit voltage (OCV) in condition A was slightly higher than that in condition B since the fuel concentration in condition A (100% $H_2$) was higher than that in condition B (31% $H_2/N_2$). In both conditions, the OCVs almost according to theoretical values. The power density in condition A was higher than that in condition B at low current density region.

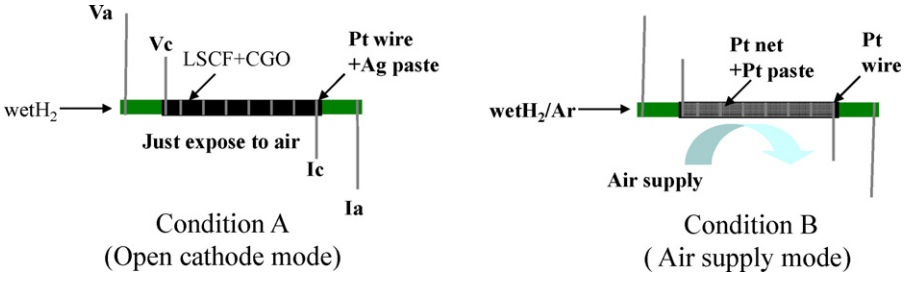


Fig. 4. The set-up deference between conditions “A” and “B”.

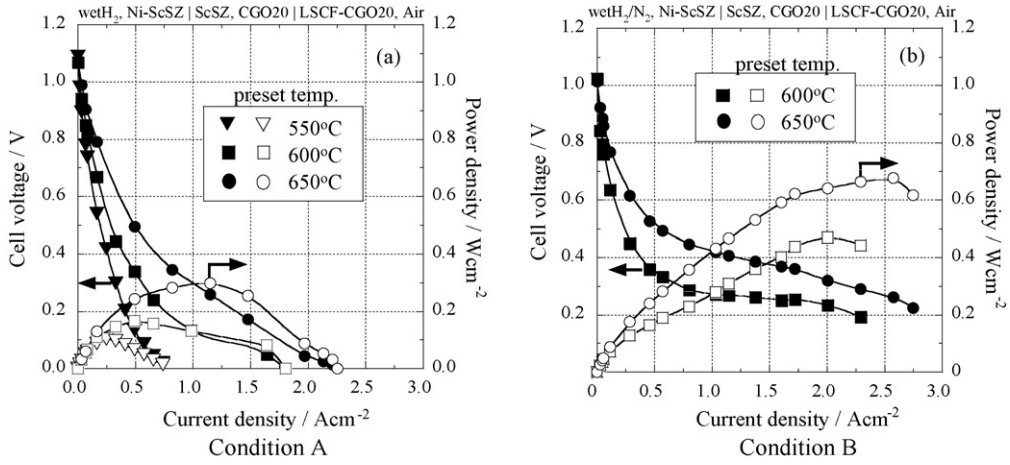


Fig. 5. Power generation curves of the micro-tubular cell at (a) condition A (open cathode mode) and (b) condition B (air supply mode).

However, the power density in condition B became higher than that in condition A over around 0.5 A cm$^{-2}$ in spite of lower fuel supply. Maximum power density at 650 °C in condition B was 0.68 W cm$^{-2}$ (at 2.6 A cm$^{-2}$, $U_f = 78\%$) while that in condition A was 0.3 W cm$^{-2}$ (at 1.2 A cm$^{-2}$, $U_f = 18\%$).

Fig. 6 shows area specific ohmic resistances and polarization resistances in each condition as a function of current density. In the region of low current density, polarization resistance was very high in both conditions (Fig. 6(b)–(d)). This result suggests activation polarization resistance is the main factor of potential drop for this cell. In spite of low ohmic resistance and enough air supply to cathode, the polarization resistance of condition B was higher than that of condition A in the low current density region. This result was probably influenced by anodic polarization. In condition B, $H_2$ concentration was controlled by $N_2$. The presence of $N_2$ on anode surface may cause high anodic polarization of condition B at the low current density range. On the other hands, it is considered that the contribution of cathode side in activation polarization is also very high although it is unknown which electrode has higher contribution on the polarization. Using the same cell, the cathode modification has done by silver dispersion to LSCF–CGO cathode, and the cathode modified cell showed the dramatic reduction of initial potential drop. It is suggested that the polarization resistance in the low current density region was caused not only by anodic polarization but also by cathodic one. In the region of high current

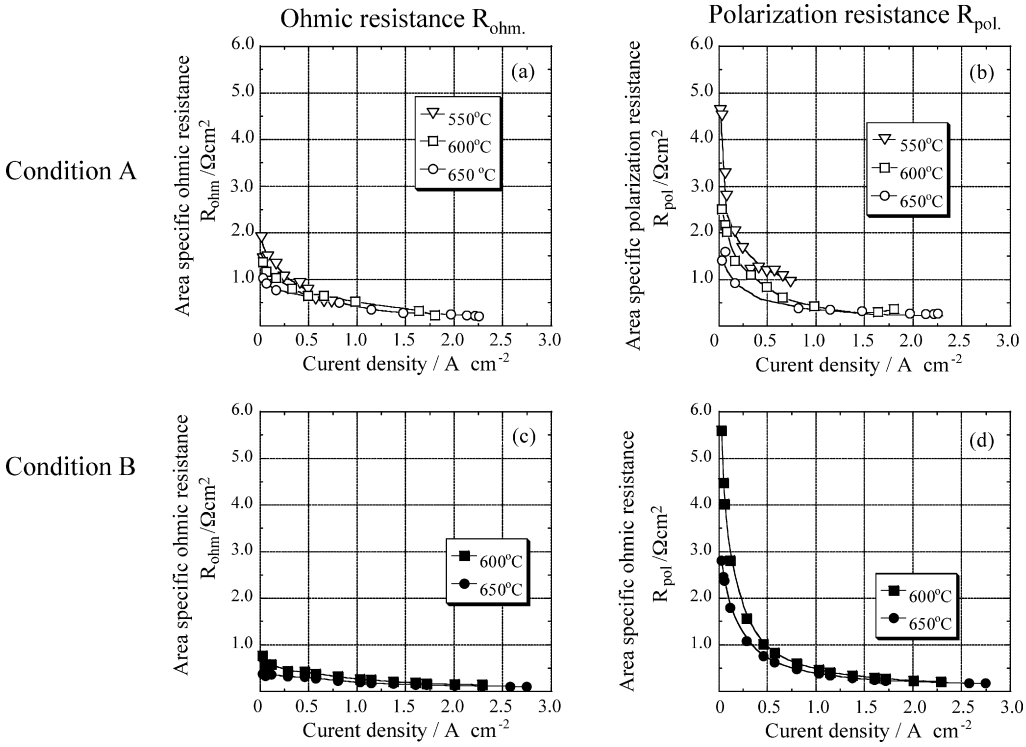


Fig. 6. Ohmic and polarization resistances as functions of current density. Change in (a) ohmic and (b) polarization resistances at condition A. Change in (c) ohmic and (d) polarization resistances at condition B.

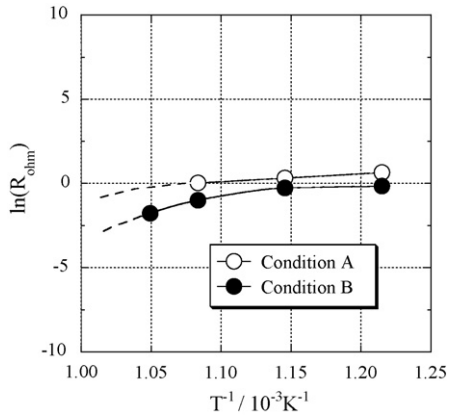


Fig. 7. Temperature dependence of cell ohmic resistance measured by current interruption method at low current region (<100 mA).

density, the polarization resistance in condition A was slightly higher than that in condition B. It was caused by inadequate air supply in condition A, and the slight difference of polarization resistance was caused large difference in the potential drop.

The ohmic resistance in condition B (Fig. 6(a)) was lower than that in condition A (Fig. 6(c)) due to better current collection on cathode side. In the imperceptible current region, below 100 mA, i.e. current density 0.057 A cm$^{-2}$, the ohmic potential drop as a function of current density was linear in both conditions, i.e. the ohmic resistance was constant, and change in cell temperature was not occur. However, the linearity between the ohmic potential drop and current density had already been lost around 0.1 A cm$^{-2}$, and an increase in current density cased a decrease in the ohmic resistances in the both conditions. Especially, the ohmic resistance in condition A vastly reduced with current density increase. It means that the cell temperature in condition A was easy to get high during the power generation compared with that in condition B.

### 4.2. The cell temperature estimation by electrochemical technique

For electrochemical temperature estimation, the temperature dependence of the cell resistance was measured by current interruption method below 100 mA as shown in Fig. 7. The cell resistance was conformed not only by current interruption method but also by impedance method at OCV using impedance analyzer (Solartron 1255WB, UK). It was conformed that there is no difference in data between these measurement methods. Obtained ohmic resistance at each current density in Fig. 6(a) and (c) was applied to Fig. 7, and the cell temperature was estimated from the ohmic resistance. The cell resistance in higher temperature region came from extrapolation. Fig. 8 shows the estimated cell temperature in (a) condition A and (b) condition B. In condition A, the estimated cell temperature was very high, and it showed over 1000 °C around the shunt current density although the preset temperature was just 600 °C or 650 °C. In contrast to the result in condition A, the estimated temperature in condition B gently increased with current density increase. The difference of estimated temperature between two conditions would be caused by the differences in current collection and the air flow. In condition A, poor current collection, i.e. high ohmic resistance including contact resistance between Pt wire and the cathode, probably caused heat generation from relatively low current region while poor air supply most likely caused additional heat generation in the high current density side. Even in condition B, the cell temperature was enhanced to pre-set temperature plus ca. 100 °C during the power generation tests. Since such anode supported micro-tubular SOFCs can generate high power in spite of the small cell size, even small resistances, i.e. ohmic and polarization resistance, will easily cause Joule heat according to $Q = Ri^2t$. At the same time, such micro tube cell geometry will also interfere with the heat radiation. These several factors probably caused the cell temperature enhancement.

In condition B, a thermo-couple was set near by the micro-tubular cell for comparison to this electrochemical technique. Fig. 9 shows (a) correlation of the temperature estimated by electrochemical technique with the temperature measured by the thermocouple in condition B and (b) photo for positional relation between measured cell and the thermo-couple. The temperature estimated by electrochemical technique ($T_{\text{eletrochem}}$) was almost proportional to the temperature measured by the thermo-couple ($T_{\text{TC}}$) although it was not in direct proportion to each other. $T_{\text{eletrochem}}$ is higher than $T_{\text{TC}}$, and 10 °C increase in $T_{\text{eletrochem}}$ corresponded to ca. 2.5 °C increase in $T_{\text{TC}}$.

Since the thermocouple keeps a little distance (ca. 2 mm) from the cell as shown in Fig. 9(b), it is expected that $T_{\text{eletrochem}}$ reflects more direct information from the cell and is close to real

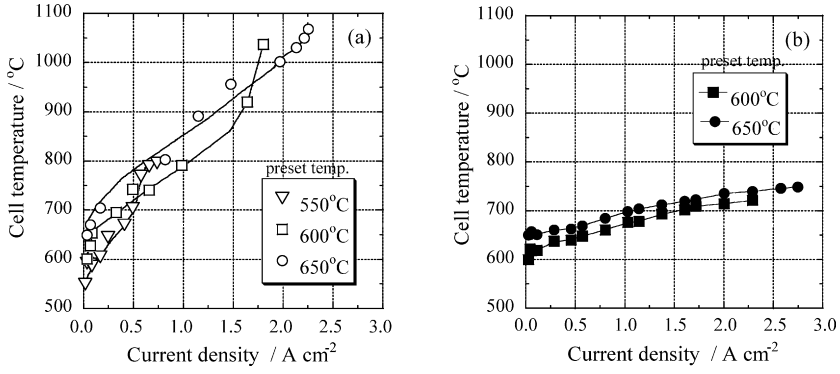


Fig. 8. The cell temperature estimated by electrochemical technique. (a) Condition A (open cathode mode) and (b) condition B (air supply mode).

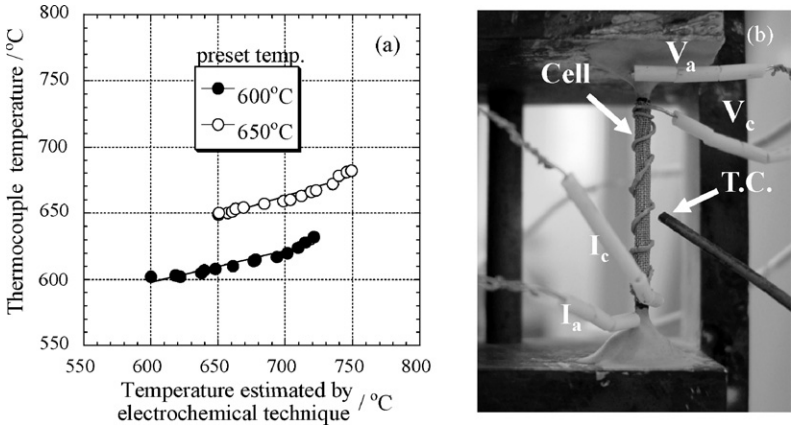


Fig. 9. (a) Correlation of estimated temperatures by electrochemical technique with the temperatures measured by the thermo-couple. (b) Positional relation between the measured cell and thermo-couple.

cell temperature. However, $T_{eletrochem}$ also contains the severall uncertainties. In these experiments, the cell resistance in higher temperature region, i.e. over 700 °C, was obtained by extrapolation as shown in Fig. 7. It means that the data reliability of $T_{eletrochem}$ in Figs. 8 and 9 may be not enough in higher temperature region although the tendency will not change. For better estimation, the cell resistance should be measured until the predictable maximum temperature during the power generation. The energization effect [8] and degradation [9] are also important factors for the precise measurement using this technique. In this experiment, data reproducibility was roughly conformed and the energization effect and degradation were not observed. However, if change in the cell status is caused by energization effect and/or degradation after cell resistance measurement as a function of temperature, the data reliability will lower.

Influence of leak current and significant changes in the potentials on electrode surfaces will be also issues for this technique. Since LSCF cathode has $P_{O_2}$ dependence in the conductivity [10,11], change in the cell resistance will be caused by diffusion/concentration over-potential on cathode side. Moreover, the electrons instead of oxide ions will start to conduct in 10ScSZ/CGO electrolyte under the condition in which high current is applied, and oxygen supply is not enough as high current density side in Fig. 8(a). Therefore, data reliability on high current side in condition A, must be low even if the cell resistance at the high temperature was measured for the more precise estimation.

Even supposing that this technique contains these difficulties, it will be very effective for cell temperature management due to direct information from real operating cells. Especially, in case of the micro-tubular SOFCs, this technique will effectively bring temperature information in a cell located at the place where the attachment of thermocouples is difficult. Some weak points would be overcome by the operational techniques. It seems to be difficult to avoid the energization effects and/or degradation completely for any kind of SOFCs. However, the influence of this problem can be minimized by regular re-measurement of temperature dependence of the cell resistance if the time dependence of these effects is no so drastic. The influence of diffusion/concentration over-potential in high current density region would be detected from *IV* curve and/or polarization measurement by ac impedance method [6,12]. If the reaction starts to show the concentration/diffusion-limited process, we will realize that the reliability of estimated temperature must start to lower. However, in usual SOFC power generation as condition "B" at around 0.5 A $cm^{-2}$, the cell ohmic resistance will basically depend solely on the temperature and the reasonable estimated temperature would be indicated.

For suitable temperature indication, the positioning for the potential sensing terminals will be also important. In this study, we just put these terminals as shown in Fig. 4. By connection of another pair of the potential sensing terminals near current terminals, the indication reliability can be improve since the cell temperature information on electric load side will be obtained by the same temperature observation technique. In the future, by some improvements for operational techniques and terminal positioning and wide verification in different situations, it is probably possible to apply this technique to cell bundles and modules.

## 5. Conclusion

We proposed new temperature observation method using electrochemical technique, and demonstrated using micro-tubular SOFCs. The fabricated micro-tubular SOFCs were operated under the two different conditions, and polarization during the power generation was measured. Cell resistance as a function temperature was also measured under fuel cell conditions. Based on the temperature dependence of cell resistance and the measured ohmic drop during the power generation, the cell temperature was estimated. The estimated cell temperature increased with increasing of the current density and was in nearly proportion to the temperature which was measured by a thermo-couple. Therefore, we concluded this method was effective for temperature management of micro-tubular structured SOFCs.

## Acknowledgements

This work had been supported by NEDO, Japan, as part of the Advanced Ceramic Reactor Project.

## References

[1] M. Prica, T. Alston, K. Kendall, in: U. Stimming, S.C. Singhal, H. Tagawa, W. Lehnert (Eds.), SOFC V, PV97-40, Proceedings Series, The Electrochemical Society, Pennington, NJ, 1997, p. 619.
[2] T. Suzuki, T. Yamaguchi, Y. Fujishiro, M. Awano, J. Electrochem. Soc. 153 (5) (2006) A925–A928.
[3] M. Awano, Y. Fujishiro, T. Suzuki, T. Yamaguchi, K. Hamamoto, Proceedings of the Seventh European SOFC Forum (CD), July 2006 (File No. B044).
[4] T. Suzuki, Y. Funahashi, T. Yamaguchi, Y. Fujishiro, M. Awano, J. Power Sources 171 (2007) 92–95.
[5] S. Hashimoto, H. Nishino, Y. Liu, K. Asano, K. Takei, M. Mori, Y. Funahashi, Y. Fujishiro, in: K. Eguchi, S.C. Singhal, H. Yokokawa, J. Mizusaki (Eds.), Solid Oxide Fuel Cells 10 (SOFC-X), ECS Trans. 7 (1) (2007) 609–613.
[6] J. Larminie, A. Dicks, Fuel Cell System Explained the second edition, Operational Fuel Cell Voltages, John Wiley and Sons, 2004 (Chapter 3).
[7] H. Iwahara, T. Esaka, H. Uchida, N. Maeda, Solid State Ionics 3/4 (1981) 359.
[8] T. Takahashi, H. Iwahara, I. Ito, Electrochemistry 38 (4) (1970) 288–293.
[9] N. Christiansen, S. Kristensen, H. Holm-Larsen, P.H. Larsen, M. Mogensen, P.V. Hendriksen, S. Linderoth, in: S.C. Singhal, J. Mizusaki (Eds.), SOFC IX, PV2005-07, Proceedings Series, The Electrochemical Society, Pennington, NJ, 2005, pp. 168–176.
[10] J.W. Stevenson, T.R. Armstrong, R.D. Carneim, L.R. Pedrson, W.J. Weber, J. Electrochem. Soc. 143–149 (1996) 2722–2729.
[11] J.A. Lane, S.J. Benson, D. Waller, J.A. Kilner, Solid State Ionics 121 (1999) 201–208.
[12] N.Q. Minh, T. Takahashi, Science and Technology of Ceramic Fuel Cells, Elsevier, 1995 (Chapters 1 and 8).